Deep tissue optical imaging of upconverting nanoparticles enabled by exploiting higher intrinsic quantum yield through use of millisecond single pulse excitation with high peak power

Liu, Haichun; Xu, Can T.; Dumlupinar, Gokhan; Jensen, Ole Bjarlin; Andersen, Peter E.; Andersson-Engels, Stefan

Published in:
Nanoscale

Link to article, DOI:
10.1039/c3nr01917a

Publication date:
2013

Document Version
Peer reviewed version

Nanoscale

Accepted Manuscript

This article can be cited before page numbers have been issued, to do this please use: H. Liu, C. T. Xu, G. Dumlupinar, O. B. Jensen, P. E. Andersen and S. Andersson-Engels, *Nanoscale*, 2013, DOI: 10.1039/C3NR01917A.

This is an *Accepted Manuscript*, which has been through the RSC Publishing peer review process and has been accepted for publication.

Accepted Manuscripts are published online shortly after acceptance, which is prior to technical editing, formatting and proof reading. This free service from RSC Publishing allows authors to make their results available to the community, in citable form, before publication of the edited article. This *Accepted Manuscript* will be replaced by the edited and formatted *Advance Article* as soon as this is available.

To cite this manuscript please use its permanent Digital Object Identifier (DOI®), which is identical for all formats of publication.

More information about *Accepted Manuscripts* can be found in the **Information for Authors**.

Please note that technical editing may introduce minor changes to the text and/or graphics contained in the manuscript submitted by the author(s) which may alter content, and that the standard **Terms & Conditions** and the **ethical guidelines** that apply to the journal are still applicable. In no event shall the RSC be held responsible for any errors or omissions in these *Accepted Manuscript* manuscripts or any consequences arising from the use of any information contained in them.

View Article Online
DOI: 10.1039/C3NR01917A

Deep tissue optical imaging of upconverting nanoparticles enabled by exploiting higher intrinsic quantum yield through using millisecond single pulse excitation with high peak power

Haichun Liu,*[a] Can T. Xu,[a] Gökhan Dumlupinar,[a] Ole B. Jensen,[b] Peter E. Andersen,[b] and Stefan Andersson-Engels[a]

Received Xth XXXXXXXXXX 20XX, Accepted Xth XXXXXXXXX 20XX
First published on the web Xth XXXXXXXXXX 200X
DOI: 10.1039/b000000x

We have accomplished deep tissue optical imaging of upconverting nanoparticles at 800 nm, using millisecond single pulse excitation with high peak power. This is achieved by carefully choosing the pulse parameters, derived from time-resolved rate-equation analysis, which result in higher intrinsic quantum yield that is utilized by upconverting nanoparticles for generating this near infrared upconversion emission. The pulsed excitation approach thus promises previously unreachable imaging depths and shorter data acquisition times compared with continuous wave excitation, while simultaneously keeping the possible thermal side-effects of the excitation light moderate. These key results facilitate means to break through the general shallow depth limit of upconverting-nanoparticle-based fluorescence techniques, necessary for a range of biomedical applications, including diffuse optical imaging, photodynamic therapy and remote activation of biomolecules in deep tissues.

1 Introduction

During the last decade, upconverting nanoparticles (UCNPs) have developed rapidly,[1–6] and show great promise as contrast agents in biological applications.[7–11] Despite tremendous improvements of UCNPs, their limited quantum yield (QY), especially at low excitation light level, is still a major concern for most potential biological applications.[12] Two interesting and powerful techniques under development are deep tissue optical imaging[13] and photodynamic therapy (PDT),[14] which both require high QY. The present low QY thus hinders the potential of these techniques to be unleashed due to prolonged data acquisition and treatment times, and shallow applicable depths.[12,15] Although low QY to some extent can be overcome by increasing the excitation light level, such improvements are fundamentally restricted for continuous wave (CW) excitation due to risks of tissue damage, regulated by the ANSI standards.[16]

Instead, the opportunity to break through the low power density limit of upconversion (UC) emission while limiting thermal effects of the excitation light is here proposed by employing pulsed excitation.[12,17,18] In addition, we realize that the applicability of UCNPs could be further boosted by utilizing single-shot excitation schemes, *i.e.*, short single pulse excitation with high peak power. Similar to multiphoton microscopy, pulsed excitation would provide high photon density during the pulse, while keeping the average power (*i.e.*, the deposited energy responsible for the heating) moderate. Due to the non-linear power density dependence of UC emission, pulsed excitation would be highly beneficial. However, two important differences exist between the UC emission and direct two-photon fluorescence. Firstly, the QY is much higher for UCNPs at low photon density rates, which constitutes one main reason for the interest in them and removes the reliance of and restriction to focal volume excitation, thus broadening their field of application.[19,20] Secondly, the excitation for UC emission relies on intermediate energy levels,[21] complicating the process. This has led to some less successful attempts to utilize pulsed excitation for UCNPs in the past.[22,23] It is thus necessary to carefully consider the excitation dynamics of UC emissions under pulsed excitation in order to utilize the higher intrinsic QY of UCNPs.

In this paper, through investigating the excitation dynamics of UC emission, we prove through simulations and experiments that significant QY increase can be achieved by using pulsed excitation with wisely selected pulse characteristics, *i.e.*, with sufficiently long pulse width and non-saturated energy transfer transitions. Our proposed scheme renders pulsed excitation an ideal excitation approach for UCNPs, especially for deeply located tissue volumes. In fact, the net QY increase enables us to implement single-shot imaging of UCNPs, shortening data acquisition time by orders of magnitude while simultaneously improving imaging depth as compared to CW

[a] *Department of Physics, Lund University, P.O. Box 118, S-221 00 Lund, Sweden. Fax: +46 46 222 4250; Tel: +46 46 222 7471; E-mail: haichun.liu@fysik.lth.se*
[b] *Department of Photonics Engineering, Technical University of Denmark, Frederiksborgvej 399, DK-4000 Roskilde, Denmark.*

View Article Online
DOI: 10.1039/C3NR01917A

excitation. These results have the potential to fundamentally broaden the applicability of UCNPs in deep tissue regions relying on diffuse light excitation, breaking the shallow-depth limitation in UCNP-based imaging.

2 Experimental

2.1 Synthesis of UCNPs

Core–shell $NaYF_4$:Yb^{3+},Tm^{3+}@$NaYF_4$ nanoparticles, synthesized through a recently reported protocol,[24] are used as a representative of UCNPs in this work.

All the chemicals were purchased from Sigma-Aldrich and used without further purification. The core nanoparticles $NaYF_4$:Yb^{3+},Tm^{3+} were first synthesized using the protocol reported in Ref. 25. In a typical synthesis, anhydrous powders of YCl_3 (0.75 mmol), $YbCl_3$ (0.25 mmol) and $TmCl_3$ (0.003 mmol) were dissolved in 6 mL oleic acid and 17 mL octadecene in a 250 mL flask at 160 °C for 30 min. After the clear solution cooling down to room temperature, 10 mL methanol solution containing 4 mmol NH_4F and 2.5 mmol NaOH was added, and the mixture was stirred for 30 min at 50 °C. The methanol was removed from the system by slowly heating it, and the resulting solution was heated to 300 °C for 1.5 h under argon atmosphere. After the mixture cooled to room temperature, the nanoparticles were precipitated with ethanol and washed with ethanol/water mixture for several times, and then redispersed in hexane to form nanoparticle suspension. The core–shell nanoparticles were subsequently produced by slightly modifying the above procedure through incorporating the prepared core nanoparticles as the seeds in the synthesis.[24] 1 mmol YCl_3 was solely used to provide rare-earth ions for the shielding layer. Other steps were kept the same as the synthesis of core nanoparticles.

2.2 Characterization and photoluminescence measurements on UCNP suspension

The as-prepared core-shell UCNPs were dispersed in hexane and used as the sample. Transmission electron microscopy (TEM) images and the density of the UCNPs were measured on a JEOL 3000F microscope equipped with a X-ray energy dispersive spectroscopy (XEDS) facility. The molar concentrations of rare earth ions were measured on a PerkinElmer Optima 8300 inductively coupled plasma optical emission spectrometer (ICP-OES). The photoluminescence measurements were performed on a sensitive spectrometer setup. A CW laser diode at 975 nm (Thorlabs L975P1WJ) was employed as the excitation source driven by a benchtop laser diode current controller (Thorlabs LDC220C), with the temperature stabilized at 25 °C. Pulsed laser light output was achieved by modulating the current controller using a function generator (Philips PM5139). The excitation power was measured using an Ophir Nova II laser power meter equipped with a photodiode sensor (Ophir PD300), while the spot size of the excitation beam was measured using a laser beam profiler (DataRay Inc. WinCamD-UCD23). The emission light was detected using a grating spectrometer (Ocean Optics QE65000) with a slit width of 50 μm. The rise profile of the 800 nm emission was recorded by an oscilloscope (Tektronix TDS520A) coupled to the output of a photomultiplier tube (Hamamatsu R928), using excitation at 975 nm from laser diode operating in the pulsed mode. All measurements were carried out at room temperature.

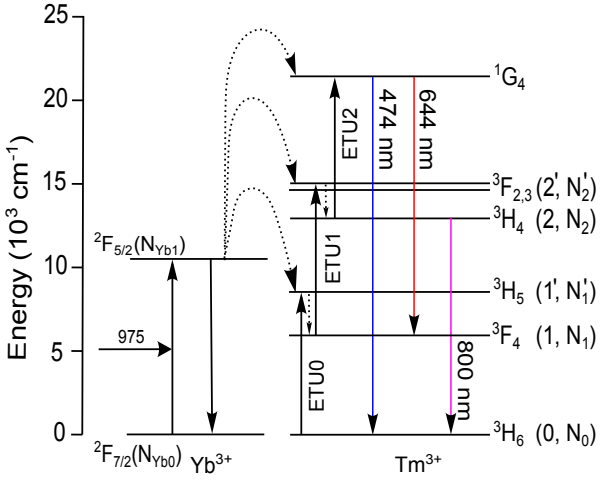

Fig. 1 Schematic energy level diagrams of Yb^{3+} and Tm^{3+} ions and the proposed UC mechanism following the excitation at 975 nm. The variables used in the text for the population densities of different levels are indicated within the parentheses.

2.3 Diffuse optical imaging using UCNPs

Diffuse optical imaging of UCNPs in liquid tissue phantom was performed either in a trans-illumination or in a epi-illumination mode. A capillary tube with an inner diameter of 2 mm, filled with UCNP suspension, was immersed within the tissue phantom to simulate the luminescent target. Excitation of the UCNPs was accomplished either by a Thorlabs L975P1WJ laser diode running in the CW mode, or by a broad area laser (Eagleyard Photonics, EYP-BAL-0980-10000-4020-CDL02-0000) operating in the pulsed mode driven by a laser diode driver (LIMO LDD50). The excitation power was measured using an Ophir Nova II laser power meter equipped with a medium power thermal laser sensor [Ophir L40(150)A-SH-V2]. A charge-coupled device (CCD) camera (Andor iXon) was used to acquire fluorescence images.

View Article Online
DOI: 10.1039/C3NR01917A

Table 1 Summary of general parameter values used in the simulations

σ (cm^2)	N_0 (cm^{-3})	N_{Yb0} (cm^{-3})	τ_{Yb1} (ms)	τ_1 (ms)	τ_2 (ms)	C_0 (cm^3/s)	C_1 (cm^3/s)	C_2 (cm^3/s)	β_1' (s^{-1})	β_2' (s^{-1})
1.69×10^{-20} [a]	1.25×10^{19} [b]	1.52×10^{21} [b]	1.32 [c]	7.43 [d]	1.49 [c]	1.6×10^{-18} [e]	6.2×10^{-16} [e]	1.6×10^{-18} [e]	1.7×10^{4} [d]	1×10^{5} [d]

[a] From Jiang *et al.*[26]; [b] Calculated (see the ESI for the calculation of ion concentrations); [c] From measurement (see Fig. S2); [d] From Ivanova *et al.*[27]; [e] Estimated from Braud *et al.*[28] and Ivanova *et al.*[27] (see the ESI for the selection of the ETU rates).

3 Results and discussion

3.1 Numerical simulations on the QY increase by the pulsed excitation

The feasibility of increasing the QY of UCNPs using pulsed excitation is first investigated through numerical simulations. The Yb^{3+}/Tm^{3+} codoped nanoparticles are used as a representative of UCNPs in this work. The UC dynamics of their major UC emission band, *i.e.*, the NIR UC emission band at around 800 nm, is modelled using the following time-resolved rate equations based on its well verified UC pathway under excitation of 975 nm light,[21,29] as shown in Fig. 1,

$$\frac{dN_{Yb1}}{dt} = \frac{\sigma\rho}{h\nu}N_{Yb0} - (C_0N_0 + C_1N_1 + C_2N_2)N_{Yb1} - \frac{N_{Yb1}}{\tau_{Yb1}}, \quad (1a)$$

$$\frac{dN_1'}{dt} = C_0N_0N_{Yb1} - \beta_1'N_1', \quad (1b)$$

$$\frac{dN_1}{dt} = \beta_1'N_1' - C_1N_1N_{Yb1} - \frac{N_1}{\tau_1}, \quad (1c)$$

$$\frac{dN_2'}{dt} = C_1N_1N_{Yb1} - \beta_2'N_2', \quad (1d)$$

$$\frac{dN_2}{dt} = \beta_2'N_2' - C_2N_2N_{Yb1} - \frac{N_2}{\tau_2}, \quad (1e)$$

where σ is the absorption cross-section of Yb^{3+} ions; ρ is the excitation power density; h is Planck's constant; ν is the frequency of the excitation light; C_0, C_1 and C_2 are the energy transfer upconversion (ETU) rates from excited Yb^{3+} ions to the Tm^{3+} ions at states 0, 1 and 2, respectively; τ_1 and τ_2 are the radiative lifetimes of Tm^{3+} ions at states 1 and 2 (non-radiative de-excitation neglected for these levels), while τ_{Yb1} is the lifetime of Yb^{3+} ions at $^2F_{5/2}$ state; β_1' and β_2' represent the non-radiative decay rates for $1' \rightsquigarrow 1$ and $2' \rightsquigarrow 2$, respectively. A power density dependent and temporally cumulative QY for the NIR UC emission in the time interval [0, t], $\eta(\rho,t)$, is defined as

$$\eta(\rho,t) \equiv \frac{\int_0^t N_2(t)/\tau_2\,dt}{\int_0^t \sigma N_{Yb0}\rho/h\nu\,dt}, \quad (2)$$

which can be calculated by numerically solving eqn (1a-e). The QY at steady state following CW excitation is given by $\eta(\rho,\infty)$.

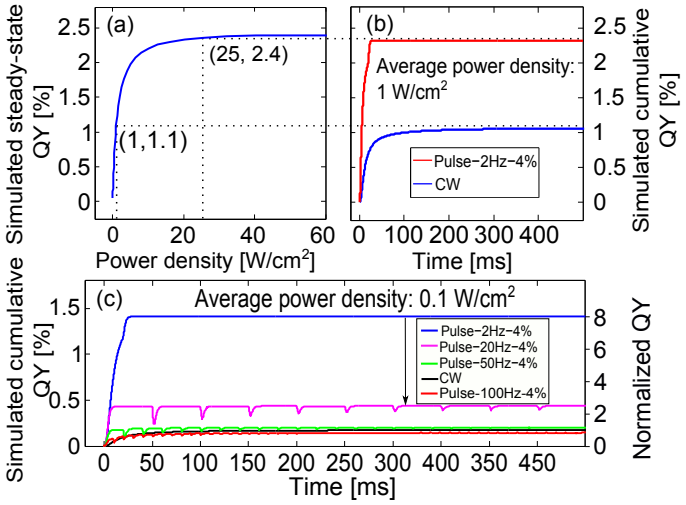

Fig. 2 (a) Simulated power density dependence of the QY of the NIR UC emission at steady state under CW excitation. (b) The temporally cumulative QYs under CW excitation and under pulsed excitaion in the first pulse period. The pulsed excitation had a duty cycle of 4% and a repetition rate of 2Hz. Both the CW and pulsed excitation approaches provided an average power density of 1 W/cm^2. (c) The temporally cumulative QYs under CW excitation and under pulsed excitation in multiple periods. The pulsed excitation had a fixed duty cycle of 4% and various repetition rates. All the excitation approaches provided the same average power density of 0.1 W/cm^2.

In the modeling, we used parameter values which were measured or calculated for the UCNPs used in the experimental work. The ion concentrations were calculated based on the TEM, ICP-OES and XEDS measurements on the UCNPs (see the ESI for the calculation of ion concentrations), and the lifetimes τ_{Yb1} and τ_2 were measured experimentally. σ, τ_1, β_1' and β_2' were taken from the literature. The power density dependent steady-state QY of the used UCNPs have been measured and reported recently in our previous work.[30] The ETU rates were thus selected on the principle of giving the best fitting of the simulated power density dependency of steady-state QY with the measured results (see the ESI for the selection of the ETU rates). Table 1 summarizes the pa-

View Article Online
DOI: 10.1039/C3NR01917A

rameter values used in the simulations. Figure 2a shows the simulated QY at steady-state conditions following CW excitation of different power densities. As seen, the QY increases with the excitation power density in a complex manner with a constant steady-state level (saturation level) at high power densities, which is consistent with experimental observations reported in the literature.[31,32]

Figure 2b presents the simulated time dependent QY under CW excitation and under pulsed excitation in the first pulse period, respectively. The CW excitation has a constant power density of 1 W/cm^2. The pulsed excitation, having a 2 Hz repetition rate and a 4% duty cycle, has power densities of 25 W/cm^2 and 0 W/cm^2 at the "on" and "off" states, respectively, thus resulting in the same average power density as the CW excitation. As shown in Fig. 2b, under CW excitation, the UC emission has a constant QY_{cw} except at the very early stage when the energy levels start to be populated due to the effect of the excitation. This constant QY_{cw} is associated with the steady state of the UC system, and given by the QY at the power density of 1 W/cm^2 in Fig. 2a. Under pulsed excitation, the QY_{pulsed} is very small at the start of the laser pulse, and then increases with time. If the length of the pulse duration allows, the QY_{pulsed} will surpass the QY_{cw}, and asymptotically approach a maximum. This maximum is restricted to the steady-state QY at the power density of 25 W/cm^2 in Fig. 2a. Clearly, the advantage of using pulsed excitation to replace the equivalent CW excitation is that the late excitation photons can be potentially used with higher energy conversion efficiency, while the cost is that the early excitation photons in each pulse period are used with lower efficiency than in the CW excitation. Through balancing the increased power density and decreased excitation duration under the same amount of energy, an overall UC signal gain (defined as the ratio of the QY_{pulsed}/QY_{cw}) can be expected .

Cumulatitive QY in multiple periods under pulsed excitation was investigated in order to estimate the influence of the pulse width on the signal gain, compared to the equivalent CW excitation. The average power density was kept at 0.1 W/cm^2 in the simulations. The pulsed excitation used throughout this study had the same duty cycle of 4% unless otherwise specified, and its repetition rate was adjusted in order to achieve different pulse widths. As illustrated in Fig. 2c, a significant UC signal gain is obtained by using pulsed excitation when the repetition rate is well below 50 Hz. For example, the signal gain by the 2 Hz square wave in the time interval of [0, 500] ms is approximately 8. The signal gain decreases with repetition rate, *i.e.*, increases with pulse width as expected. When the repetition rate is even higher, *e.g.*, up to 100 Hz, the signal generated by the pulsed excitation becomes slightly smaller than that generated by equivalent CW excitation. In addition, it should be noted that the signal gain decreases with the applied power density. When the average power density is increased to 1 W/cm^2, the signal gain decreases to 2, as shown in Fig. S3. This can be ascribed to the gradual saturation property of UC emission, indicated in Fig. 2a.

Although the parameter values were carefully calculated or modified in the simulations so that it gives the best fitting between the measured and simulated steady-state QY power density dependency, the modeling is not an accurate description of the real UC system. Due to the lack of accuracy and precision data for such values, it is difficult to evaluate the uncertainty of the simulated results. However, the influence of the variation of parameter values on the simulated signal gain was investigated, with the results for the change of ETU rates shown in Fig. S4. In each comparison, one ETU rate among others was adjusted across the two orders of magnitude around the value listed in Table 1, while two other ETU rates remained unchanged. All simulated results confirm that UC emission enhancement effect can be achieved by using pulsed excitation with a considerably long pulse duration when the energy transfer transitions are not saturated by the applied power density, as long as the emission originates from a multi-stepwise photon upconversion process. The only difference exists in the extent of the signal gain. It is worth mentioning that the simulated signal gain has a strong dependence on the change of the ETU rate C_1 rather than C_0 and C_2, as shown in Fig. S4. This can be explained by the fact that the balancing power density of UCNPs is highly dependent on C_1.[30] Above this power density, the UCNPs would behave more linearly in emitting upconverted photons upon NIR excitation,[30] leading to decreased signal gain by using pulsed excitation.

3.2 Quantum yield increase by pulsed excitation in UCNP suspension

In order to experimentally validate the gain in UC signal due to the pulsed excitation predicted by the simulations in Section 3.1, experiments were carried out on colloidal stable UCNPs. Core–shell $NaYF_4$:Yb^{3+},Tm^{3+}@$NaYF_4$ UCNPs were dispersed in hexane and used as the sample. The prepared UCNPs emit the major UC emission bands at around 800 nm under excitation of 975 nm light, as shown in Fig. 3, assigned to the transition $^3H_4 \rightarrow {}^3H_6$ of Tm^{3+} ions.[29] Other weaker UC emission bands at around 450 nm, 474 nm and 644 nm originate from the transitions of Tm^{3+} ions $^1D_2 \rightarrow {}^3F_4$, $^1G_4 \rightarrow {}^3H_6$ and $^1G_4 \rightarrow {}^3F_4$, respectively.[29] The inset of Fig. 3 shows the TEM image of the prepared core–shell UCNPs. The nanoparticles were spherical in shape with an average diameter of 42 nm. The core nanoparticles prior to coating had an average diameter of 32 nm (see Fig. S1 in the ESI).

The intensities of the NIR UC emission under CW excitation and pulsed excitation (square wave) were measured. The pulsed excitation had a fixed duty cycle of 4% and different pulse widths. The average power density of the excitation light

View Article Online
DOI: 10.1039/C3NR01917A

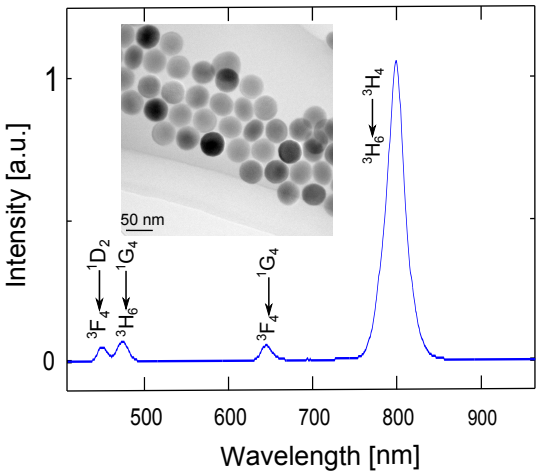

Fig. 3 The upconversion spectrum of core–shell $NaYF_4$:Yb^{3+},Tm^{3+}@$NaYF_4$ nanoparticles under excitation of a CW 975 nm laser diode, measured at a power density of 125 W/cm^2. The inset shows the TEM image of the prepared core–shell UCNPs.

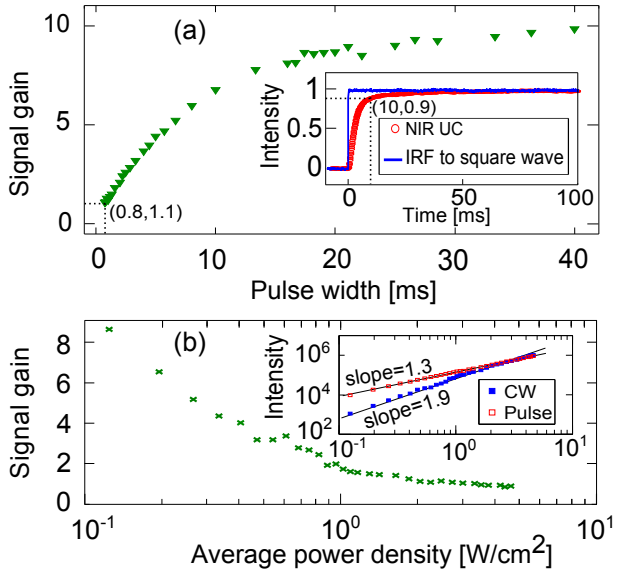

Fig. 4 (a) The NIR UC signal gain by the pulsed excitation with different pulse widths. The data were measured with an average excitation power density of 0.12 W/cm^2. Inset: The response of the NIR UC emission to a square-wave excitation with IRF denoting instrument response function. (b) The dependence of the NIR UC signal gain by the pulsed excitation on the average power density. The pulsed excitation was set to have a 20 ms pulse width and 2 Hz repetition rate. Inset: The average power density dependence of the NIR UC emission intensity under CW and pulsed excitations.

was kept at 0.12 W/cm^2. As shown in Fig. 4a, a signal gain, monotonically increasing with pulse width, was obtained by using the pulsed excitation even with a pulse duration as short as 0.8 ms. When the pulse width reaches 20 ms, the gain is as high as 8.7. It is noteworthy to point out that the required pulse width for the UC signal gain in the present case (~0.8 ms) is much shorter than the rise time of the UC emission (*i.e.*, approximately 10 ms, as shown in the inset of Fig. 4a), dominated by the lifetime of the intermediate level $^3F_4$ of Tm^{3+} ions. This is different from previous predictions reported in the literature,[12,18] and makes the pulsed excitation approach even more flexible to use due to a broader pulse width window for QY increase.

The dependence of the gain in UC signal on the applied power density was also investigated using a square-wave excitation with a 20 ms pulse width and 2 Hz repetition rate. Figure 4b shows the UC signal gain by the pulsed excitation at various average excitation power densities, where a decreasing trend with increasing excitation power densities is clearly seen. At the minimum power density investigated (~0.12 W/cm^2), the signal gain is approximately 8.7, while at the maximum power density (~4.65 W/cm^2), the UC signal generated by the pulsed excitation is slightly weaker than that generated by the CW excitation. The UC emission intensity dependence on the excitation power density under pulsed excitation exhibits a smaller slope than under the CW excitation, as shown in the inset of Fig. 4b, which could explain the signal-gain trend above.

The amplification effect of increasing the excitation power density here essentially originates from the non-linear power density dependence of the UC emission. Thus, a higher-order power density dependence would result in a larger UC signal gain. This is confirmed by the measurements on the blue (at 474 nm) and red (at 644 nm) UC emissions, both generated through a three-photon excitation process. They exhibit significantly larger signal gains than the NIR UC emission at any given average power density, as shown in Fig. 5. In view of this, we foresee that pulsed excitation can be employed to increase the applicability of recently implemented migration-mediated UC emissions from such as Eu^{3+} and Tb^{3+} ions in biological applications, due to their high-order multi-stepwise excitation nature *via* excited Tm^{3+} ions.[33] At present, their applications in such areas are challenged due to their low QYs.

It is worth mentioning that the usefulness of pulsed excitation for increasing the QY of UC emissions is not merely limited to Yb^{3+}/Tm^{3+} codoped UCNPs. Instead, it is a general scheme for enhancing UC emissions and would work in diverse UCNPs with different dopants if the characteristic of the pulsed excitation light is wisely tailored. In addition, as different UCNPs exhibit different optical characteristics, proper characterization will make it possible to accurately predict the performance of UCNPs in general under pulsed excitation.

View Article Online
DOI: 10.1039/C3NR01917A

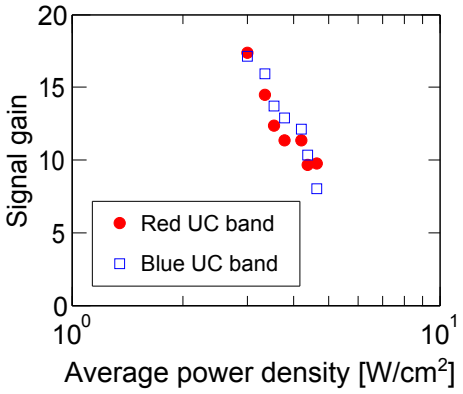

Fig. 5 The dependency of the blue (at 474 nm) and red (at 644 nm) UC signal gains by the pulsed excitation on the average power density. The pulsed excitation was set to have a pulse width of 20 ms and a repetition rate of 2 Hz.

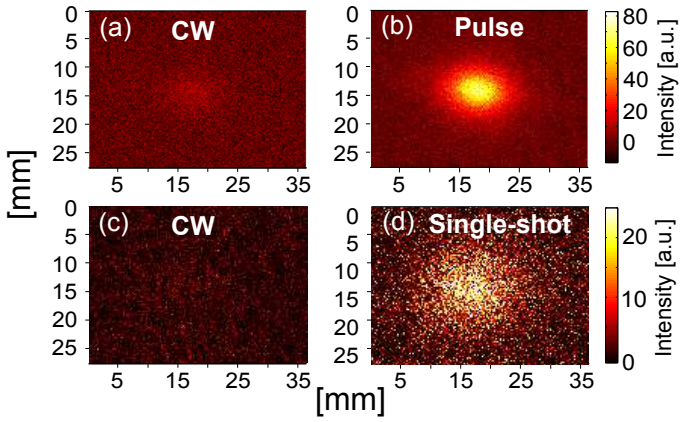

Fig. 6 The NIR UC emission images taken for a luminescent inclusion located at a depth of 10 mm under the (a) CW and (b) pulsed excitation, detected in a trans-illumination geometry. The average power density was 1.2 W/cm^2, and the exposure time was 10 s for both excitation approaches. The NIR UC emission images taken for a luminescent inclusion located at a depth of 13 mm under the (c) CW and (d) 50 ms single pulse excitation, detected in a epi-illumination geometry. Both excitation sources provided the maximum permissible power density allowed by ANSI standard for exposure to human skin. The exposure time was 10 s for the CW excitation and 1 s for the single pulse excitation.

3.3 Single-shot imaging of UCNPs

When UCNPs are used as contrast agents in diffuse optical imaging, the imaging depth is usually shallow due to the very low QY of UC emissions at the low fluence rates found in deep tissues.[12] The pulsed excitation constitutes an ideal approach for exciting deeply located UCNPs, since the UC emissions can be enhanced without consuming more excitation energy than an equivalent CW source, thus not increasing the thermal side-effects of the excitation light. This would in turn lead to higher image quality and larger imaging depth.

The merit of using pulsed excitation light to image deeply located UCNPs was subsequently tested in a liquid tissue phantom. The phantom, made of water, intralipid and ink, was characterized by photon time-of-flight spectroscopy (pTOFS)[34] and determined to have reduced scattering coefficient $\mu_s' = 10.1$ cm^{-1} and absorption coefficient $\mu_a = 0.52$ cm^{-1} at 975 nm, hence mimicking skin tissue properties. Its thickness was 17 mm. A glass tube with an inner diameter of 2 mm, containing the colloidal core–shell UCNPs ($c = 1$wt%), was inserted into the phantom as the luminescent inclusion to mimic a UCNP-labeled target, *e.g.*, a tumor inside real tissue. CW excitation and pulsed excitation, having 20 ms pulse duration and 2 Hz repetition rate, at 975 nm were applied, respectively. The average power density impinging on the surface of the tissue phantom was 1.2 W/cm^2 for both excitation approaches. The excitation source and the detector were positioned in a trans-illumination geometry. A more detailed description of the experimental setup is found in Ref. 32. When buried at a depth of 10 mm from the source, the luminescent inclusion was barely detectable under CW excitation even with an exposure time of 10 s, as shown in Fig. 6a. However, by using pulsed excitation, the signal-to-background ratio was significantly increased by a factor of approximately 7 under the same detection conditions, as illustrated in Fig. 6b. An obvious implication is that the data acquisition time can be drastically reduced whilst maintaining the signal quality equivalent to CW excitation. Moreover, it is notable that the maximum imaging depth can be increased to 15 mm for pulsed excitation (data not shown).

The QY of UC emission can be further optimized by using single pulse excitation, through which even higher power density can be achieved. For instance, the maximum permissible power density for exposure to human skin at 975 nm is 17.4 W/cm^2 for a repetitive pulse excitation with a pulse width of 20 ms and a repetition rate of 2 Hz, while the number for a 50 ms single pulse is as high as 36.9 W/cm^2,[16] referring to section 8 in the ESI. Such a strong single pulse with a pulse width longer than the rise time of the UC emission enables the UCNPs to be used in a very efficient way in terms of energy conversion. This excitation approach would improve the imaging ability of using UCNPs without violating the ANSI standard, which is a fundamental limit for bio-imaging.

The feasibility of single-shot imaging was experimentally investigated. A 50 ms single pulse providing excitation power density of 36.9 W/cm^2 was used. When the luminescent inclusion was placed at a depth of 13 mm into the phantom, it

View Article Online
DOI: 10.1039/C3NR01917A

could be relatively well detected using the single pulse excitation with a detector integration time of 1 s, even using an epi-illumination imaging setup described in Ref. 17, as shown in Fig. 6d. Nevertheless, when the CW laser was used for excitation, also outputting the maximum permissible power density by ANSI standard on the same illumination area, *i.e.*, 709.6 mW/cm^2, referring to section 8 in the ESI, the inclusion was not detectable at all even with a much longer integration time of 10 s, as shown in Fig. 6c. Obviously, the integration time for the single pulse excitation can be shortened to 50 ms still without loss in the UC signal quality, as long as the excitation source and the detector are synchronized. The results demonstrated here, although preliminary, show great potential of single-shot excitation in UCNP-guided deep tissue optical imaging.

4 Conclusions

In conclusion, significant QY increase in UCNPs is achieved by using pulsed excitation. This is supported theoretically by the study of the UC dynamics based on time resolved rate equations. Such QY increase enables us to implement single-shot imaging of UCNPs in deep tissues. Pulsed excitation thus constitutes an ideal excitation approach for UCNPs, as the shallow imaging limit can be overcome and data acquisition time can be drastically shortened by applying this excitation scheme. The pulsed excitation approach will greatly increase the applicability of UCNPs not only in diffuse optical imaging but also in many other biomedical applications, such as photodynamic therapy and remote activation of biomolecules in deep tissues.[35,36] It is worth mentioning that metallic nanostructures are reported to be effective in enhancing UC emissions owing to their local field enhancement effect by surface plasmonic coupling.[37] We envisage that the combination of the pulsed excitation approach and metallic nanostructures could become a major scheme of using UCNPs in the diffuse light regime, due to the synergistic effect in increasing the excitation power density. In addition, this study provides a general method for promoting the applications of nonlinear fluorophores (including UCNPs and triplet-triplet annihilation based upconverters[38]) at low light conditions by increasing the excitation fluence rate through a limited illumination area.

Acknowledgments

S. Fredriksson, F. Olsson, A. Gisselsson, and P. Kjellman are gratefully acknowledged for the help with the synthesis of the UCNPs and ICP-OES measurement. M. E. Messing and L. R. Wallenberg are acknowledged for the help with the TEM and XEDS measurements. B. Thomasson is acknowledged for the help in the single-shot imaging experiment. S. Johansson and A. Shaharin are acknowledged for the help with the pTOFS measurements. We thank D. Kroon and D. Guenot for the assistance in the laser power measurement, and J. Axelsson and P. Svenmarker for their helpful discussions. This work was supported by a grant from the Swedish Research Council (grant No. 621-2011-4265) and a Linneaus grant to the Lund Laser Centre.

References

1 X. Wang, J. Zhuang, Q. Peng and Y. D. Li, *Nature*, 2005, **437**, 121–124.
2 H.-X. Mai, Y.-W. Zhang, R. Si, Z.-G. Yan, L.-D. Sun, L.-P. You and C.-H. Yan, *J. Am. Chem. Soc.*, 2006, **128**, 6426–6436.
3 J.-C. Boyer, L. A. Cuccia and J. A. Capobianco, *Nano Lett.*, 2007, **7**, 847–852.
4 E. M. Chan, C. Xu, A. W. Mao, G. Han, J. S. Owen, B. E. Cohen and D. J. Milliron, *Nano Lett.*, 2010, **10**, 1874–1885.
5 F. Wang, Y. Han, C. S. Lim, Y. Lu, J. Wang, J. Xu, H. Chen, C. Zhang, M. Hong and X. Liu, *Nature*, 2010, **463**, 1061–1065.
6 F. Zhang, G. B. Braun, A. Pallaoro, Y. Zhang, Y. Shi, D. Cui, M. Moskovits, D. Zhao and G. D. Stucky, *Nano Lett.*, 2012, **12**, 61–67.
7 L. Wang, R. Yan, Z. Huo, L. Wang, J. Zeng, J. Bao, X. Wang, Q. Peng and Y. Li, *Angew. Chem. Int. Ed.*, 2005, **44**, 6054–6057.
8 S. F. Lim, R. Riehn, W. S. Ryu, N. Khanarian, C. K. Tung, D. Tank and R. H. Austin, *Nano Lett.*, 2006, **6**, 169–174.
9 M. Nyk, R. Kumar, T. Y. Ohulchanskyy, E. J. Bergey and P. N. Prasad, *Nano Lett.*, 2008, **8**, 3834–3838.
10 H. Päkkilä, M. Ylihärsilä, S. Lahtinen, L. Hattara, N. Salminen, R. Arppe, M. Lastusaari, P. Saviranta and T. Soukka, *Anal. Chem.*, 2012, **84**, 8628–8634.
11 M. Yu, F. Li, Z. Chen, H. Hu, C. Zhan, H. Yang and C. Huang, *Anal. Chem.*, 2009, **81**, 930–935.
12 C. T. Xu, Q. Zhan, H. Liu, G. Somesfalean, J. Qian, S. He and S. Andersson-Engels, *Laser Photonics Rev.*, 2012, DOI:10.1002/lpor201200052.
13 J. Zhou, Z. Liu and F. Li, *Chem. Soc. Rev.*, 2012, **41**, 1323–1349.
14 N. M. Idris, M. K. Gnanasammandhan, J. Zhang, P. C. Ho, R. Mahendran and Y. Zhang, *Nat. Med.*, 2012, **18**, 1580–1585.
15 F. C. J. M. van Veggel, C. Dong, N. J. J. Johnson and J. Pichaandi, *Nanoscale*, 2012, **4**, 7309–7321.
16 Laser Institute of America, *Americal National Standard for Safe Use of Lasers*; *in ANSI Z136.1-2000* (Laser Institute of America, Orlando, Florida, 2000).
17 C. T. Xu, N. Svensson, J. Axelsson, P. Svenmarker, G. Somesfalean, G. Chen, H. Liang, H. Liu, Z. Zhang and S. Andersson-Engels, *Appl. Phys. Lett.*, 2008, **93**, 171103.
18 Q. Zhan, S. He, J. Qian, H. Cheng and F. Cai, *Theranostics*, 2013, **3**, 303–316.
19 H. Liu, C. T. Xu and S. Andersson-Engels, *Opt. Lett.*, 2010, **35**, 718–720.
20 P. Svenmarker, C. T. Xu and S. Andersson-Engels, *Opt. Lett.*, 2010, **35**, 2789–2791.
21 F. Auzel, *Chem. Rev.*, 2004, **104**, 139–173.
22 L. M. Maestro, E. M. Rodriguez, F. Vetrone, R. Naccache, H. L. Ramirez, D. Jaque, J. A. Capobianco and J. G. Solé, *Opt. Express*, 2010, **18**, 23544–23553.
23 C. F. Gainer, G. S. Joshua, C. R. De Silva and M. Romanowski, *J. Mater. Chem.*, 2011, **21**, 18530–18533.
24 H.-S. Qian and Y. Zhang, *Langmuir*, 2008, **24**, 12123–12125.
25 Z. Li and Y. Zhang, *Nanotechnology*, 2008, **19**, 345606.
26 X. P. Jiang, Z. M. Yang, T. Liu and S. H. Xu, *J. Appl. Phys.*, 2009, **105**, 103113.

View Article Online
DOI: 10.1039/C3NR01917A

27 S. E. Ivanova, A. M. Tkachuk, A. Mirzaeva and F. Pelle, *Opt. Spectrosc.*, 2008, **105**, 228–241.
28 A. Braud, S. Girard, J. L. Doualan, M. Thuau, R. Moncorg'e and A. M. Tkachuk, *Phys. Rev. B*, 2000, **61**, 5280–5292.
29 G. Chen, T. Y. Ohulchanskyy, R. Kumar, H. Ågren and P. N. Prasad, *ACS Nano*, 2010, **4**, 3163–3168.
30 H. Liu, C. T. Xu, D. Lindgren, H. Xie, D. Thomas, C. Gundlach and S. Andersson-Engels, *Nanoscale*, 2013, **5**, 4770–4775.
31 R. Page, K. Schaffers, P. Waide, J. Tassano, S. Payne, W. Krupke and W. Bischel, *J. Opt. Soc. Am. B*, 1998, **15**, 996–1008.
32 C. T. Xu, P. Svenmarker, H. Liu, X. Wu, M. E. Messing, L. R. Wallenberg and S. Andersson-Engels, *ACS Nano*, 2012, **6**, 4788–4795.
33 F. Wang, R. Deng, J. Wang, Q. Wang, Y. Han, H. Zhu, X. Chen and X. Liu, *Nat. Mater.*, 2011, **10**, 968–973.
34 T. Svensson, E. Alerstam, D. Khoptyar, J. Johansson, S. Folestad and S. Andersson-Engels, *Rev. Sci. Instrum.*, 2009, **80**, 063105.
35 C. J. Carling, F. Nourmohammadian, J. C. Boyer and N. R. Branda, *Angew. Chem. Int. Ed.*, 2010, **49**, 3782–3785.
36 M. K. G. Jayakumar, N. M. Idris and Y. Zhang, *Proc. Natl. Acad. Sci. U.S.A.*, 2012, DOI:10.1073/pnas.1114551109.
37 S. Schietinger, T. Aichele, H.-Q. Wang, T. Nann and O. Benson, *Nano Lett.*, 2010, **10**, 134–139.
38 S. Baluschev, T. Miteva, V. Yakutkin, G. Nelles, A. Yasuda and G. Wegner, *Phys. Rev. Lett.*, 2006, **97**, 143903.

View Article Online
DOI: 10.1039/C3NR01917A

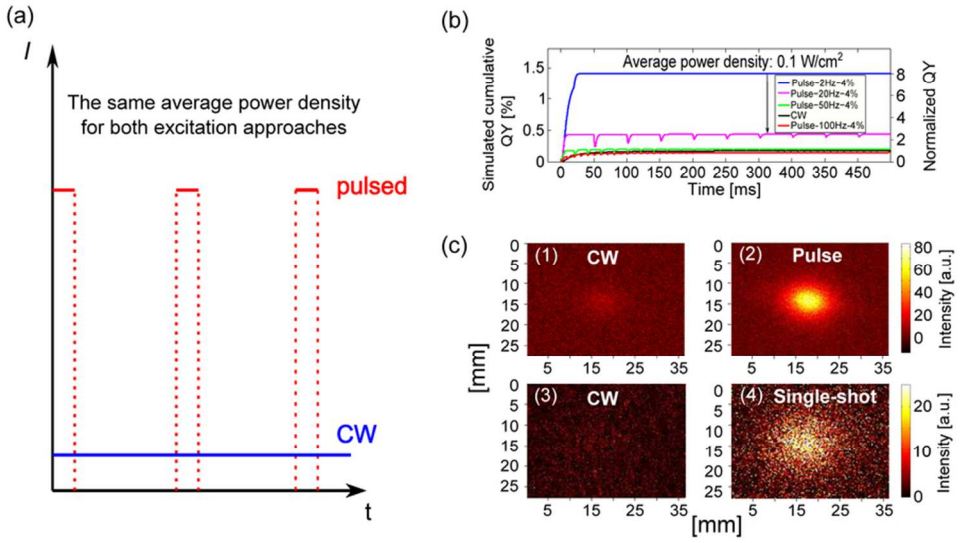

Significant quantum yield increase can be achieved by using pulsed excitation compared to the equivalent continuous excitation providing identical average power density, which enables single-shot imaging of upconverting nanoparticles in deep tissues.
40x21mm (600 x 600 DPI)